11th International Symposium on Turbulence and Shear Flow Phenomena (TSFP11)
Southampton, UK, July 30 to August 2, 2019

# STEREO PIV MEASUREMENTS OF VERTICAL VARIATION OF LOCAL VENTILATION RATES FOR A GENERIC BUILDING EXPOSED TO AN ATMOSPHERIC BOUNDARY LAYER

**Vasiliki Pappa**
School of Mechanical Engineering
National Technical University of Athens
9 Heroon Polytechniou, 15780 Zografou, Greece
Email: vaswpappa@gmail.com

**Apostolis Langidis**
School of Mechanical Engineering
National Technical University of Athens
9 Heroon Polytechniou, 15780 Zografou, Greece
Email: aostl@hotmail.com

**Marinos Manolesos**
College of Engineering, Swansea University
Bay Campus, Fabian Way
Swansea, Wales, SA1 8EN, UK
Email: marinos.manolesos@swansea.ac.uk

**Demetri Bouris**
School of Mechanical Engineering
National Technical University of Athens
9 Heroon Polytechniou, 15780 Zografou, Greece
Email: dbouris@fluid.mech.ntua.gr

## ABSTRACT

A new set of Stereo Particle Image Velocimetry (Stereo PIV) measurements is presented for the calculation of the cross-ventilation rate distribution along the height of a building. The experiments focus on a generic cubic building, oriented normal to the flow, for two different turbulent atmospheric boundary layers. Along the middle of the upstream and downstream faces, a single vertical opening was present. Measurements were performed at planes normal to the flow and within 0.05H (H is the building height) of the upstream and downstream faces. Thus, the local ventilation rate was calculated along the openings, providing increased accuracy compared to previous studies and empirical relations (orifice equation). Significant spatial and temporal variation of the ventilation rates is found and correlation between the ventilation rate, horseshoe vortex, stagnation point location and upstream flow is investigated.

## INTRODUCTION

Building cross-ventilation is a complicated flow problem, in part due to the dependence on local and upstream wind properties, including shear and turbulence. The prediction of building ventilation rates is a subject of ongoing research with significant implications regarding building energy consumption and indoor air quality. Empirical methods based on the orifice equation cannot be applied to openings located in series, on the grounds that the pressure distribution along the aperture is not constant and the foretelling results are ambiguous (Murakami, 1991). In cross-ventilation, the flow has a «choice» (flow through or past), which is not taken into account with the orifice equation (Kobayashi et al.,2010). In order to enhance the understanding of the cross-ventilation mechanism, experimental studies have been conducted using wind tunnels. These studies either apply single-point intrusive techniques e.g. hot-film (Murakami et al., 1991; Kato et al., 1992) or tracer gas methods (Tominaga and Blocken, 2015). The adoption of non-intrusive techniques like Particle Image Velocimetry (PIV) is still limited (Karava et al., 2011) whilst Stereo PIV is rare (Cao et al., 2014).

In this study, we investigate the characteristics of the velocity field in a cross-ventilated, cubic, single-zone building, exposed to two different upstream turbulent boundary layers. The vertical openings are a novel approach in order to study the vertical variation of the flow on the upstream and downstream faces (Manolesos et al.,2018). Combined with the proximity of the measurement planes to the openings, this permits overall insight with regard to the vertical variation of local ventilation rates and investigation of its correlation to flow characteristics.

## EXPERIMENTAL SETUP

### Measurement Techniques

The experiments were performed in the large test section (2.5m×3.5m×12m) of the National Technical University of Athens wind tunnel. The cubic building model had a height of H=110 mm while a 22x22 mm hollow column was included at the centre of the cube, to conceal pressure tap tubing for surface pressure measurements, which, however, are not included in the present study (see Manolesos et al., 2018). The cubic building is made from 5 mm thick plexiglass sheets and the slot shaped openings are 90x6 $mm^2$, corresponding to 4.5% of each of the vertical sides' area. Irwin-type spires (Irwin, 1981) and ground-mounted roughness elements were installed, upstream of the test section, to generate a scaled atmospheric boundary layer flow. The four Irwin-type spires had a height of 1800 mm, a front face base-width of 200 mm and were spaced 900 mm apart from each other. The roughness elements were 50 mm cubes at a staggered spacing of D=200 mm.

Two different upstream boundary layers were produced, using different combinations of roughness element positioning, in order to vary mean velocity profiles, surface shear stress, turbulence intensity and length scales. The two upstream boundary layers are distinguished as Low shear (A) and High shear (B) boundary layers, respectively (Figure 1).

Hot-wire anemometry was used to measure the boundary layer profiles with a measuring time of 105 s at 10 kHz sampling rate, for each point. The two boundary layers had similar mean velocity values at the cube height, but overall different turbulence intensity and mean velocity profiles. Specifically, the resulting aerodynamic roughness length and friction velocity were: $z_o$=2.6 mm, u*=0.37 m/s for the High shear profile and $z_o$=0.12 mm, u*=0.2 m/s for the Low shear one. The velocity at the cube height was $U_H$=3.2 m/s for High shear and $U_H$=3.5 m/s for Low shear inflow, which corresponds to a Reynolds number of ≈24000, well over the suggested limit for Reynolds number independence of the flow (Castro and

Robins, 1977; Lim et al., 2007). The model scale factor was calculated, according to Cook (1978) at 1:400, up to a height of 3H where the integral length scale was $L_{ux} \approx 2.5H$ for both profiles. The velocity well above the simulated boundary layer was $U_\infty \approx 5.1$ m/s for both cases. According to VDI (2000), the turbulence intensity up to the building model height (H), corresponds to that of a flow over rough terrain for High shear inflow, i.e. park, suburban area while for Low shear inflow, it corresponds to a flow over moderately rough terrain, i.e. grassland or farmland.

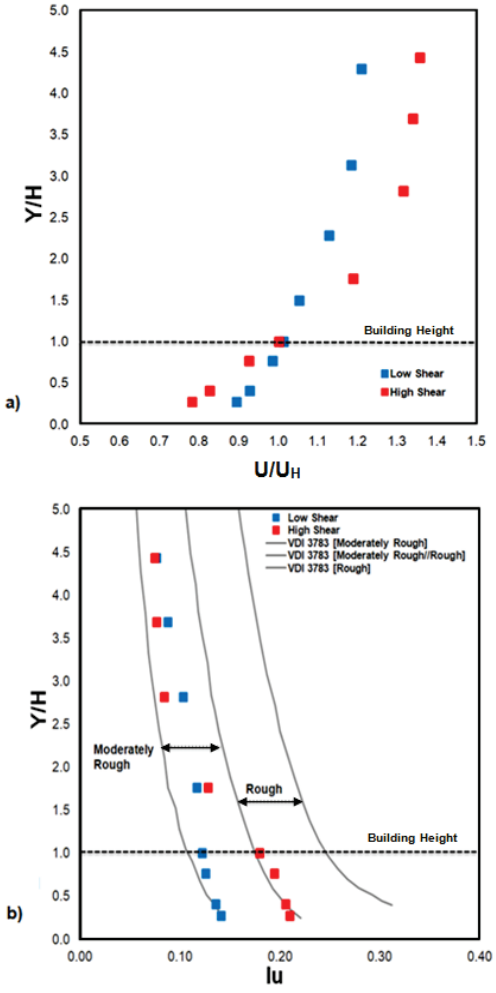


Figure 1.a) Mean velocity ($U/U_H$) and b) Streamwise turbulence intensity ($I_u$) profiles for the Low and High shear boundary layers.

Stereo PIV measurements were performed to determine the three-component velocity field in the planar region illuminated by a laser light sheet. The system consisted of two TSI Powerview Plus 4Mpixel cameras connected to a TSI Inc. system and software with a double pulse Nd:YAG laser with a nominal energy of 200 mJ per pulse. Seeding of the flow was achieved by the use of a commercial droplet generator (TSI model 9307) which produced olive oil droplets of diameter 1-2 μm. Measurement planes were sampled at a rate of 0.5Hz. Previously (Manolesos et al., 2018) measurements were performed on planes parallel to the flow (A, B, C in Figure 2) but proximity to the cube surface was limited to 0.09H (≈1cm) due to reflections. In this study, measurements were made in the planes normal to the air flow, in front of and behind the cubic model (D, E in Figure 2), within a distance of 0.05H (≈0.5cm) from the vertical building faces. The schematic of the Stereo PIV installation is depicted in Figure 3.

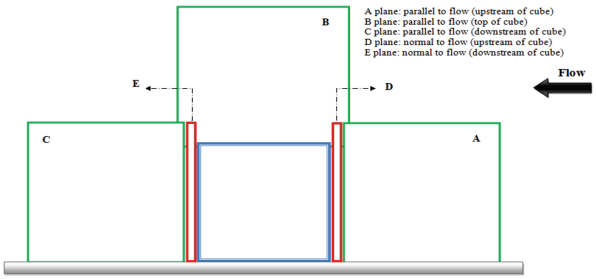


Figure 2.Side view of Stereo PIV measurements planes (A,B,C) (Manolesos et al.,2018) and (D,E) of present study.

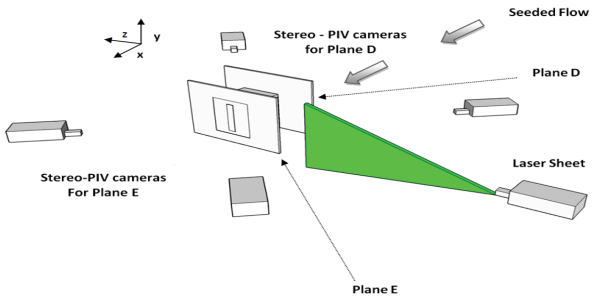


Figure 3. Schematic of the Stereo PIV installation for planes D and E, normal to the flow.

A pulse separation time of 85 μsec was used, as higher values would increase the measurement noise and make peak detection more difficult. The corresponding minimum resolved velocity (the velocity corresponding to displacement of 0.1px, Foucaut et al. 2004; Westerweel, 2000]) was equal to 0.13 m/s, so any values below this should not be trusted. For all planes, the number of spurious vectors was always below 5% and spurious vectors were replaced using a 3×3 vector local mean. The particle displacement was in all cases less than 1/4 of the 32 × 32px interrogation area and a 50% overlapping was used.

## RESULTS

The measured mean velocity in the main flow direction on the upstream plane D (see Figure 3) is presented in Figure 4, for the two different upstream boundary layers. The streamwise velocity profiles are plotted along the vertical building apertures, i.e. from y = 0.1H to y = 0.9H from the ground. The cube height (H) and the freestream velocity ($U_\infty$) have been used as reference values to non-dimensionalise the results. Table 1 lists the test cases and presents the mean ventilation rates that are calculated from these profiles using equation:

$$\int_{y=0.1H}^{y=0.9H} U(y)\, bdy \qquad (1)$$

where U(y) is the mean streamwise velocity across the width of the opening at height y from the ground, b is the aperture width and the aperture height is h=0.8H. It is the Low shear boundary layer that leads to higher streamwise velocities in the plane just upstream the cube. This in turn leads to higher ventilation rates (Table 1). Mass balance verification has been performed for the present measurements and the differences in flow rates

calculated from the upstream and downstream measurement planes is below 5% for both boundary layers.

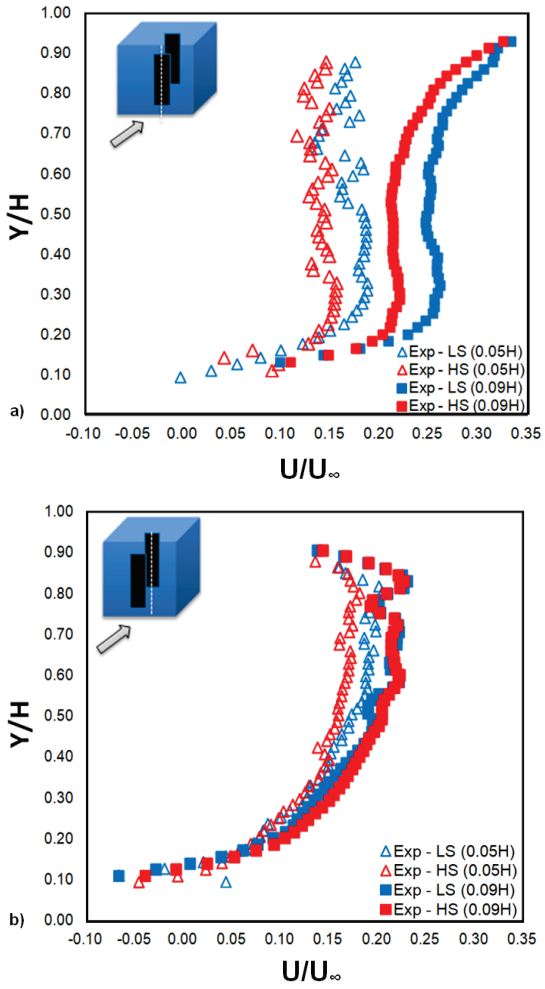


Figure 4.Non-dimensional mean streamwise velocity profiles along the vertical openings of the cubic building for Low and High shear, a) upstream opening (plane D) and b) downstream opening (plane E).

Table 1. Comparison between experimental results of local ventilation rates from past and present test cases.

| Upstream BL | Measurement Distance From Opening | Mean Flow Rate [$10^{-4}$ $m^3/s$] |
|---|---|---|
| Low Shear | 0.05H | 4.18 |
| High Shear | 0.05H | 3.48 |
| Low Shear | 0.09H | 7.00 |
| High Shear | 0.09H | 6.20 |

The flow rate standard deviation variation along the aperture has also been calculated locally i.e. for ten equally spaced regions of the openings, each with a height of $\Delta y=h/10$ (Figure 5). The variability is significantly larger near the ground (Figure 5).

In Figure 6, time series of the instantaneous ventilation rate for the lowest $\Delta y$ aperture in plane D are plotted for the Low and High Shear cases. The high variability and the frequent sign changes the ventilation rate (i.e. from inflow to outflow) are obvious in both cases. It is posited that this is related to the horseshoe vortex instability.

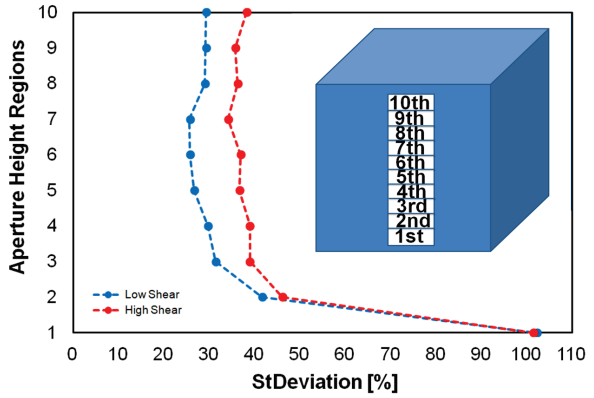


Figure 5. Standard deviation of local mean flow rate for Low and High shear, in plane D.

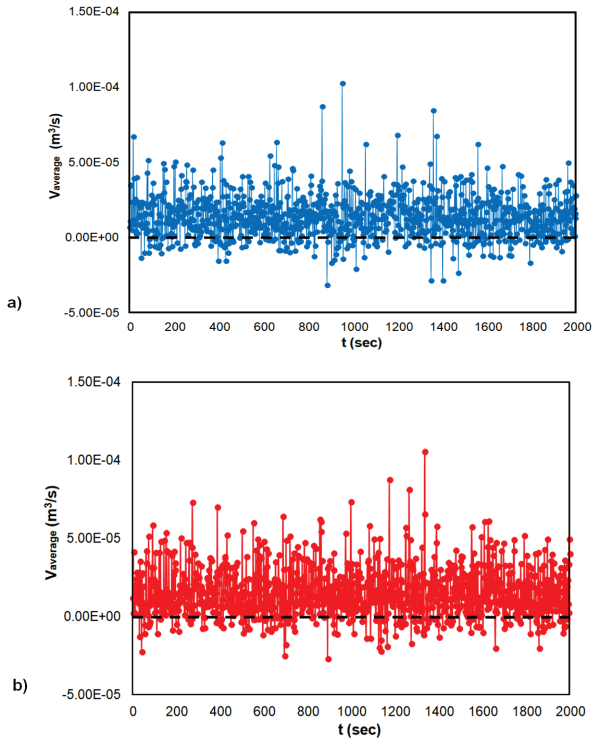


Figure 6. Mass flow variation for the lowest aperture region on plane D for both a) Low and b) High shear inflow.

In the present study, horseshoe vortex mobility has been investigated using the Q-criterion (Jeong and Hussain, 1995) and the vortex centre was defined as the position of the Q-criterion maximum value in each of the 1000 measured instants. Figure 7 displays the locations of instantaneous Q-criterion maximum values for the Low and High shear inflow cases, for planes D and E, upstream and downstream of the building, respectively. In Figure 7a-b, plane D, these points correspond to the centres of the horseshoe vortex on either side of the building. In Figure 7c-d, the horseshoe vortex seems to be weak and the appearing variability of maximum Q values may be related to the downstream toroidal vortex. In order to examine the correlation between the horseshoe vortex centre location and the velocities along the openings, and therefore ventilation rates, Pearson's correlation coefficients were calculated among three parameters, on plane D: Q-criterion (representing the horseshoe vortex intensity), $V'_{average}(y)$ (local mean flow rate) and r (Euclidean distance between the upstream corner on the ground and the horseshoe vortex

centre). However, all of these correlations were found to be weak, not exceeding values of 0.2 all along the aperture height.

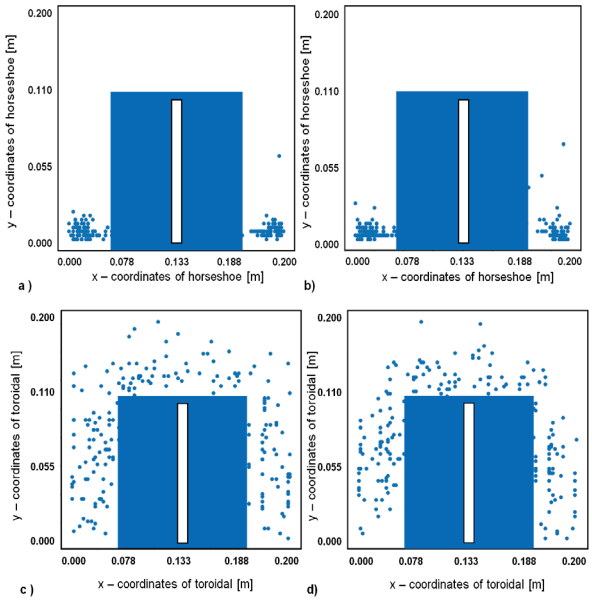


Figure 7. Positions of maximum instantaneous Q criterion values, in plane D, for a) Low shear and b) High shear inflow, and in plane E, for c) Low shear and d) High shear inflow.

Following the horseshoe vortex variability, the variability of the position of the stagnation point was also examined. Although the stagnation point is strictly defined on the solid surface, for a measurement plane that is close to the surface, an indication of the stagnation point has been considered as the attachment node of the in-plane flow lines.

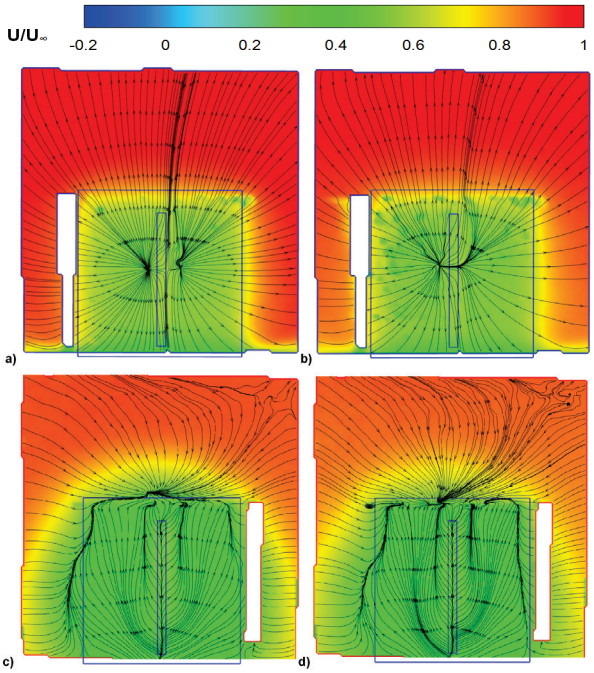


Figure 8. In-plane streamlines and contours of the average, non-dimensional mean streamwise velocities $U/U_\infty$, on plane D for a) Low shear and b) High shear, on plane E for c) Low shear and d) High shear.

The mobility of the stagnation point is reproduced in Figures 8-9, which represent contours of non-dimensional streamwise velocities $U/U_\infty$, for planes D and E, for Low and High shear inflow cases. The figures comprise contours of the streamwise velocity and in-plane streamlines from the mean velocity field (Figure 8, as calculated from the total snapshots) and from two random, instantaneous velocity fields (Figure 9). Figures 8a-b show an expected upstream face pattern with in plane flow lines emanating from where the stagnation region is expected i.e. just higher than mid-height. Figure 9 gives a clear picture of significant mobility of the attachment node of the in-plane flow paths, indicating a similar behavior of the stagnation region (circled in the figure).

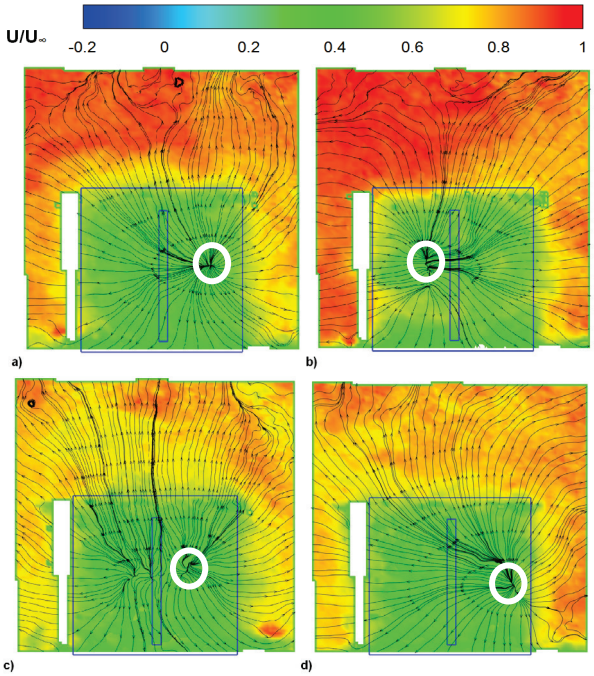


Figure 9. In-plane streamlines and contours of instantaneous, non-dimensional streamwise velocities $U/U_\infty$, from two random snapshots, on plane D for a-b) Low shear and c-d) High shear. Indicated stagnation points are circled.

The stagnation point coordinates were defined as the position of minimum velocity magnitude in every snapshot (total: 1000 snapshots), for both inflow boundary layers and both measurement planes. The locations of the stagnation points in Plane D are shown in Figure 10 for both upstream boundary layers.

The strong variation of the stagnation point position induced interest to calculate Pearson correlation's coefficients between $V'_{average}(y)$ (mean flow rate variation) and r, the variation of the Euclidean distance between the stagnation point position and each of the 10 points along the height of the opening, presented in Figure 5. Correlations along the height of the opening are presented in Figure 11. It seems that the ventilation rate through the top and bottom of the opening is affected by the proximity of the stagnation point, with a correlation reaching values of $R \approx -0.3$. The ventilation rate at mid-height does not seem to be significantly affected by the stagnation point motion. This is slightly below the mean stagnation point position (see Figure 10) and is also a region where mean ventilation rates are relatively high.

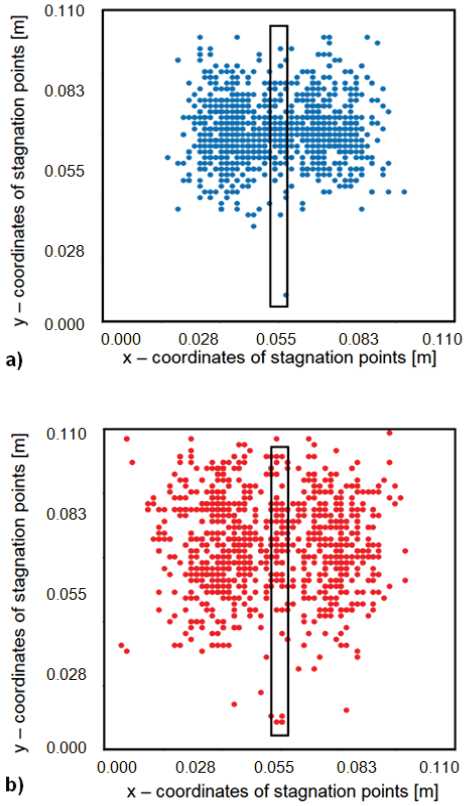


Figure 10. Stagnation points' positions on plane D, for a) Low and b) High shear inflow.

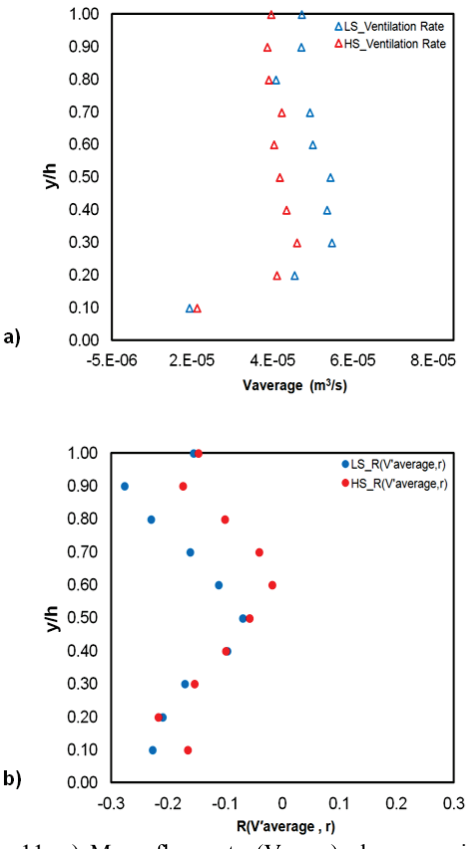


Figure 11. a) Mean flow rate ($V_{average}$) along opening height and b) Pearson correlation coefficient, R($V'_{average}$, r) between local mean flow rate and respective distance from stagnation point. Low and High shear inflow, plane D.

According to Sandberg et al. (2015), the identification of the locations of stagnation points is necessary because they are the distribution points for the air flowing out over the windward façade. Therefore, for flow through openings, the locations of the openings relative to the location of the stagnation point(s) are important. The latter proposal is partly verified as the stagnation point position is a sufficient condition for the flow field but, at least based on the present measurements, correlation between stagnation point locations and mean ventilation rates seems to be weak.

Further exploring the significant variation in the stagnation point positions, information from previous measurements (Manolesos et al., 2018) taken in a plane parallel to the flow, was processed. Specifically, taking into account the measured data in plane A (Figure 2), and at a distance of 1.5H upstream of the building location, the fluctuation of the upstream flow direction was calculated. The fluctuation of the angle (θ) in the xy plane, between the streamwise velocity component ($U_x$) and the velocity vector in this plane ($U_{xy}$) was calculated, as well as the fluctuation of the angle (φ) in the xz plane, between the streamwise velocity component ($U_x$) and the velocity vector in this plane $U_{xz}$. These angles are depicted in Figure 12.

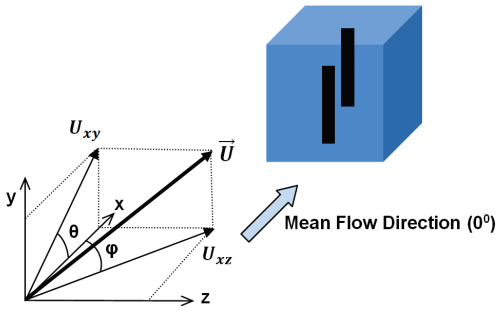


Figure 12: Definition of flow direction angles in upstream flow ($0^0$).

Table 2 lists the results of the angle variation. It is notable that, generally, for Low and High shear, the angle standard deviation in the xy plane is approximately $3^0$ to $4^0$, while for the xz plane, its standard deviation varies between 4.5 to 5.3 degrees, respectively. If one takes into account the extremes, then instantaneous values of over 20 degrees were measured. Starting at a distance of 1.5H upstream of the cube face, this change in flow direction leads to a span wise distance of dz = 1.5H·tan(20) = 0.55H, which is more than half the cube width. Another perspective is that it corresponds to an instantaneous cube orientation of $20^0$. This is a plausible explanation for stagnation point variation: the more intense the variability in upstream flow direction, the stronger the stagnation point mobility in the building façade.

Table 2: Standard deviation and extreme minimum-maximum values of flow direction angle for upstream, Low & High shear inflow. Angles in xy plane and xz plane.

| | LS xy plane | LS xz plane | HS xy plane | HS xz plane |
|---|---|---|---|---|
| **stDev ($^0$)** | 3.014 | 4.456 | 4.196 | 5.288 |
| **min-max ($^0$)** | (-4 to 15) | (-12 to 19) | (-7 to 23) | (-14 to 21) |

## CONCLUSIONS

An experimental analysis of the flow and ventilation rates for a cubic building with vertical openings exposed to two different upstream boundary layers has been performed.

The mean ventilation rates calculated for the Low shear boundary layer, are higher than for the case of High shear inflow, as expected.

The measurement proximity parameter is a key factor for the accuracy of the measurements with differences of ~50% between measurements at distances of 0.05H(~0.5cm) and 0.09H(~1cm) from the openings. Mean ventilation rates measured closer to the openings adhere to mass balance between the upstream and downstream openings with differences below 5%.

Measurements of the local ventilation rate show significant fluctuation, especially near the ground. Correlation coefficients between horseshoe vortex location, vortex intensity and mean vertical ventilation rates were found to be weak for both boundary layers. A stronger correlation was found between the position of the stagnation points on the upstream cube face and the local ventilation rates.

The position of the stagnation points shows significant fluctuation and it has been shown that this can be related to the variability of the upstream flow direction, due to turbulence.

## ACKNOWLEDGEMENTS

This work was financially supported by a scholarship from the Eugenides Foundation. The first author gratefully acknowledges this support.

## REFERENCES

Cao X., Liu J. and Jiang N. 2014"An Overview of the Applications of Particle Image Velocimetry for Indoor Airflow Field Measurement" *Proceedings of the 8th International Symposium on Heating, Ventilation and Air Conditioning: Volume 3:Building Simulation and Information Management* Springer Berlin Heidelberg Berlin, Heidelberg pp 223-231.

Castro I. and Robins A., 1977, "The flow around a surface mounted cube in uniform and turbulent streams". J. Fluid Mech., Vol. 79, No. 2, pp. 307-335.

Cook N J. 1978, "Determination of the model scale factor in wind-tunnel simulations of the adiabatic atmospheric boundary layer". Journal of Wind Engineering and Industrial Aerodynamics, Vol 2(4), pp 311-321

Foucaut J. M., Miliat B., Perenne N., and Stanislas M., "Characterization of different PIV algorithms using the EUROPIV synthetic image generator and real images from a turbulent boundary layer," in Particle Image Velocimetry: Recent Improvements, Springer, 2004, pp. 163–185

Irwin, H. (1981). The design of spires for wind simulation. Journal of Wind Engineering and Industrial Aerodynamics, 7(3), 361-366.

Jeong J. and Hussain F., (1995). On the identification of a vortex. *Journal of Fluid Mechanics, 285*(-1), 69-94.

Karava P., Stathopoulos T. and Athienitis A., 2011 "Airflow assessment in cross ventilated buildings with operable facade elements" Building and Environment 46 (2011) 266-279.

Kato S. Murakami, S., Mochida A., Akabayashi S., and Tominaga, Y. 1992, "Velocity pressure field of cross ventilation with open windows analyzed by wind tunnel and numerical simulation" *Journal of Wind Engineering and Industrial Aerodynamics* Vol 44 No 1 1992 pp 2575-2586.

Kobayashi T., Sandberg M., Kotani H., Claessson L., (2010) "Experimental investigation and CFD analysis of cross-ventilated flow through single room detached house model". Building and Environment 45(2010) 2723-2734.

Lim, Hee Chang, Castro I. P., and Hoxey R. P., 2007. "Bluff bodies in deep turbulent boundary layers: Reynolds-number issues." J. Wind Eng. Ind. Aerodyn. Vol 571 pp. 97-118.

Manolesos M., Gao Z., Bouris D.,(2018) "Experimental investigation of the atmospheric boundary layer flow past a building model with openings". Building and Environment, DOI: 10.1016/j.buildenv.2018.05.049.

Murakami, S. 1991 "Wind tunnel test on velocity-pressure field of cross-ventilation with open windows" *ASHRAE Transactions* Vol 97 1991 pp 525-538.

Murakami S., Kato S., Akabashi S., Mizutani K., Kim Y-D. "Wind tunnel test on velocity-pressure field of cross-ventilation with open windows". ASHRAE Transactions 1991;(97)(1):525-38.

Sandberg M., Mattson M., Wigö H., Hayati A., Claesson L., Linden E., Khan M.A(2015)"Viewpoints on wind and air infiltration phenomena at buildings illustrated by field and model studies", Building and Environment 92 (2015) 504-517.

Tominaga Y. Blocken B. (2015) "Wind tunnel experiments on cross-ventilation flow of a generic building with contaminant dispersion in unsheltered and sheltered conditions". Building and Environment 92 (2015) 452-461.

VDI, (2000). Environmental Meteorology - Physical Modelling of Flow and Dispersion Processes in the Atmospheric Boundary Layer - Application of Wind Tunnels. VDI guideline 3783 Part 12.

Westerweel J., "Theoretical analysis of the measurement precision in particle image velocimetry," Exp. Fluids, vol. 29, no. 1, pp. S003–S012, 2000.